POTENTIAL CLINICAL SIGNIFICANCE

Nanomedicine: Nanotechnology, Biology, and Medicine
11 (2015) 1387–1397

nanomedicine
Nanotechnology, Biology, and Medicine

Feature Article

nanomedjournal.com

Nanoformulation of antiretroviral drugs enhances their penetration across the blood brain barrier in mice

Luisa Fiandra, PhD[b], Miriam Colombo, PhD[c], Serena Mazzucchelli, PhD[b], Marta Truffi, PhD[a], Benedetta Santini, BPharm[c], Raffaele Allevi, CLT[a], Manuela Nebuloni, PhD[a], Amedeo Capetti, MD[b], Giuliano Rizzardini, MD[b], Davide Prosperi, PhD[c,d], Fabio Corsi, MD[a,*]

[a]*Dipartimento di Scienze Biomediche e Cliniche "Luigi Sacco", Università di Milano, Milano, Italy*
[b]*Ospedale L. Sacco, Milano, Italy*
[c]*Dipartimento di Biotecnologie e Bioscienze, Università di Milano-Bicocca, Milano, Italy*
[d]*Laboratorio di Biofisica e Nanomedicina, Polo Tecnologico, Fondazione Don Gnocchi IRCCS-ONLUS, Milan, Italy*

Received 24 June 2014; accepted 19 March 2015

Abstract

Eradication of virus by sanctuary sites is a main goal in HIV management. The central nervous system (CNS) is a classic model of sanctuary where viral replication occurs despite a complete viral suppression in peripheral blood. In recent years, nanotechnologies have provided a great promise in the eradication of HIV from the CNS. We hereby demonstrate for the first time that the structurally complex antiretroviral drug enfuvirtide (Enf), which normally is unable to penetrate the cerebrospinal fluid, is allowed to cross the blood brain barrier (BBB) in mice by conjugation with a nanoconstruct. Iron oxide nanoparticles coated with an amphiphilic polymer increase Enf translocation across the BBB in both *in vitro* and *in vivo* models. The mechanism involves the uptake of nanoconjugated-Enf in the endothelial cells, the nanocomplex dissociation and the release of the peptide, which is eventually excreted by the cells in the brain parenchyma.

From the Clinical Editor: Despite the success of cocktail therapy of antiretroviral drugs, the complete eradication of HIV remains elusive, due to existence of viral sanctuary sites. The authors showed in this study that an antiretroviral drug complexed with iron oxide nanoparticles and coated with PMA amphiphilic polymer crosses the blood brain barrier. Furthermore, there was significant anti-viral activity. The results would aid further drug designs to eradicate HIV.

Key words: HIV sanctuaries; Enfuvirtide; Blood brain barrier; PMA-coated nanoparticles

Background

Current antiretroviral treatment regimens suppress plasma HIV-1 RNA and DNA below detectable levels in a consistent proportion of subjects.[1] However, functional cure and eradication are still beyond our possibilities. One obstacle to such goals is represented by the difficulty to achieve therapeutic antiretroviral concentrations within sanctuary sites where HIV-1 has been shown to compartmentalize. Such sites include the genital tract, the gut-associated lymphoid tissue, the lymph nodes, tissue macrophages and the central nervous system (CNS).[2-4] In particular, the CNS is considered one of the most important viral reservoirs. This is mainly due to the presence of macrophages that promote the inflammatory escalation with subsequent astrogliosis and neurodegeneration, thus establishing the so-called NeuroAIDS,[5] responsible for neurocognitive disorders

Abbreviations: AF660, Alexa Fluor 660; BBB, blood brain barrier; CNS, central nervous system; DLS, dynamic light scattering; ECM, endothelial cell medium; Enf, enfuvirtide; Epf, epifluorescence; FI, fluorescence intensity; FD40, FITC-Dextran 40; FITC, fluoresceinamine; HAART, highly active anti-retroviral therapy; ICP-OES, inductively coupled plasma optical emission spectrometry; MRP, multidrug resistance-associated protein; P_{app}, apparent permeability coefficient; PBS, phosphate buffer saline; PFA, paraformaldehyde; PMA, poly(isobutylene-alt-1-tetradecene-maleic anhydride); RBMVECs, rat brain microvascular endothelial cells; RT, room temperature; SE, standard errors; SEM, scanning electron microscopy; TEM, transmission electron microscopy; TEER, transendothelial electrical resistance.

This work was supported by the Fondazione Regionale per la Ricerca Biomedica (FRRB), NanoMeDia Project (Regione Lombardia and "L. Sacco" Hospital), and by the "Fondazione Romeo ed Enrica Invernizzi".

M.T. acknowledges "Centro di Microscopia Elettronica per lo sviluppo delle Nanotecnologie applicate alla medicina" (CMENA, University of Milan) for the postdoctoral fellowship.

*Corresponding author at: Dipartimento di Scienze Biomediche e Cliniche "Luigi Sacco", Università di Milano, Milano, Italy.
E-mail address: fabio.corsi@unimi.it (F. Corsi).

http://dx.doi.org/10.1016/j.nano.2015.03.009
1549-9634/

with different grades of severity (AIDS dementia complex). From a clinical point of view, NeuroAIDS is a real challenge since the blood brain barrier is poorly crossable by most antiretroviral drugs.[2]

In the effort toward viral eradication, one of the most promising strategies is to treat this latent-T cell reservoir, so that resting cells may be induced to release virions and reactivate,[6-9] while preventing HIV-1 entry in uninfected CD4+ T cells. With this aim it would be important to design new therapeutic strategies to direct antiretroviral drugs in these HIV sanctuaries, both to reduce T-cell mediated delivery of the virus into the sanctuaries and to directly act on HIV-sensitive CD4+ cells inside these sites (*i.e.* microglial cells of brain)[4].

Nanotechnology is an emerging multidisciplinary field that has the potential to offer a radical change in the treatment and monitoring of HIV/AIDS.[10-13] The potential advantages in using nanoparticles for HIV infection treatment include the capacity to incorporate, encapsulate, or conjugate a variety of drugs in order to target specific cell populations, grant long-term drug release, and penetrate into sanctuary sites. With regard to the CNS, the employment of nanotechnology could allow antiretroviral drugs to effectively reach this reservoir,[14] thus preventing the replication of the virus and reducing the damages induced by the infection.

In current clinical practice, the first-line antiretroviral therapy is generally constituted by a combination of two nucleoside reverse transcriptase inhibitors (NRTI) with a non-nucleoside reverse transcriptase inhibitor (NNRTI), such as a protease inhibitor or an integrase inhibitor. Conversely, fusion inhibitors are much less used because of some well-known limitations such as production time and costs, difficult administration (subcutaneous injection twice daily) and adverse effect profile.[15] Therefore, fusion inhibitors are only used in case of resistance or failure of the HAART. Enfuvirtide (Fuzeon™ from Roche Laboratories Inc. and Trimeris Inc.) is a 36-amino acid peptide that targets multiple sites in gp41, a HIV glycoprotein responsible for the fusion with CD4+ cells.[16-18] Enfuvirtide (Enf) inhibits HIV-1-mediated cell-cell fusion and transmission of cell-free virus while it does not have substantial activity against HIV-2.[19-22] Because of its unfavorable pharmacological profile, with a half life of approximately 2 h and a high molecular weight (4.5 kDa), Enf is particularly indicated to provide a proof of concept of the improved access of antiretroviral drug to HIV sanctuaries by nanoformulation. Indeed, Enf does not penetrate the BBB because of its complex structure, and is therefore not detectable in cerebrospinal fluid (CSF).[23]

Aim of our study is to demonstrate the ability of iron oxide nanoparticles coated with PMA amphiphilic polymer (MYTS) to enhance the permeation of a high-weighted molecule, such as Enf, across the BBB both in *in vitro* and *in vivo* models, and propose a mechanism for drug delivery across the endothelium.

Methods

Nanoparticle design

Magnetic nanoparticles (MNP) were synthesized by solvothermal decomposition in organic solvent from organometallic precursors according to Park et al. protocol.[24] MNP were transferred to water phase using a fluorescent labeled amphiphilic polymer (PMA).[25] Fluorescent-PMA was obtained with fluoresceinamine 1.0 M (0.5 mL in DMSO) was added to a 0.5 M PMA in $CHCl_3$ (5 mL) and the mixture was left overnight at RT. Part of this solution (20 μL) was added to MNP (1.5 mg in $CHCl_3$). The organic solvent was evaporated and sodium borate buffer (SBB, pH 12, 20 mL) was added obtaining a stable nanoparticle dispersion which was concentrated in Amicon tubes (100 kDa filter cutoff) by centrifuging at 3500 rpm for 20 min. The nanoparticles were washed twice with water resulting in green labeled PMA-coated nanoparticles highly soluble in aqueous media (MYTS). MYTS were reacted with an amino-linker useful for Enf immobilization on the nanoparticles. Enf was previously labeled with AF660 dye (Invitrogen, Carlsbad, CA) according to manufacturer's protocol. The final double labeled Enf-MYTS are schematically represented in Figure 1, *A*.

Characterization of the BBB in vitro model

The setting of the BBB *in vitro* model, based on a co-colture of RBMVECs and astrocytes, is described in Supplementary materials. Before each experiment, we checked the trans-BBB electrical resistance by an EVOM2 Epithelial tissue Volt/Ohmmeter connected to an Endohm-24SNAP cup (WPI, Germany), obtaining a suitable value on 90% of the inserts. Moreover, the trans-BBB apparent permeability coefficient of FITC-Dextran 40 (FD40) was determined by measuring the flux of the molecule from the upper to the lower chamber of three BBB systems at 1 h, 2 h and 3 h from the addition of 1 mg mL^{-1} FD40 in the upper compartment. The flux through the RBMVECs single layer or through the empty insert was used as control. The amount of FD40 recovered in the lower compartment was determined spectrofluorimetrically and the P_{app} was calculated from the mean flux (see Supplementary materials).

In vitro trans-BBB permeation

The permeation of (AF660)Enf, (FITC)MYTS or (AF660)Enf-MYTS(FITC) across the BBB was assessed on the *in vitro* model described above, using four inserts for each experimental condition. The two formulations were added to the upper chamber and, after 4 or 7 h of incubation, a defined volume of ECM was collected by both the upper and the lower chambers. The fluorescence intensity of the samples was measured spectrofluorimetrically. For an exact comparison between the trans-BBB permeation of free and MYTS-conjugated Enf (5 μg mL^{-1}), the FI of the two formulations was used for normalization, and the final amount of Enf-MYTS in the upper chamber was 0.1 mg mL^{-1}.

ICP-OES was also used to quantify the amount of MYTS iron in the collected samples.

Reported results are representative of one of three independent experiments.

Plasma concentration measurements in mice

Plasma concentration of free or conjugated Enf was determined upon intravenous injection of AF660-labeled Enf (0.2 μg g^{-1} body weight) or Enf-MYTS (12.5 μg g^{-1} body weight) in Balb/c mice. We treated four mice per experimental condition and repeated the experiment twice (for a total of eight

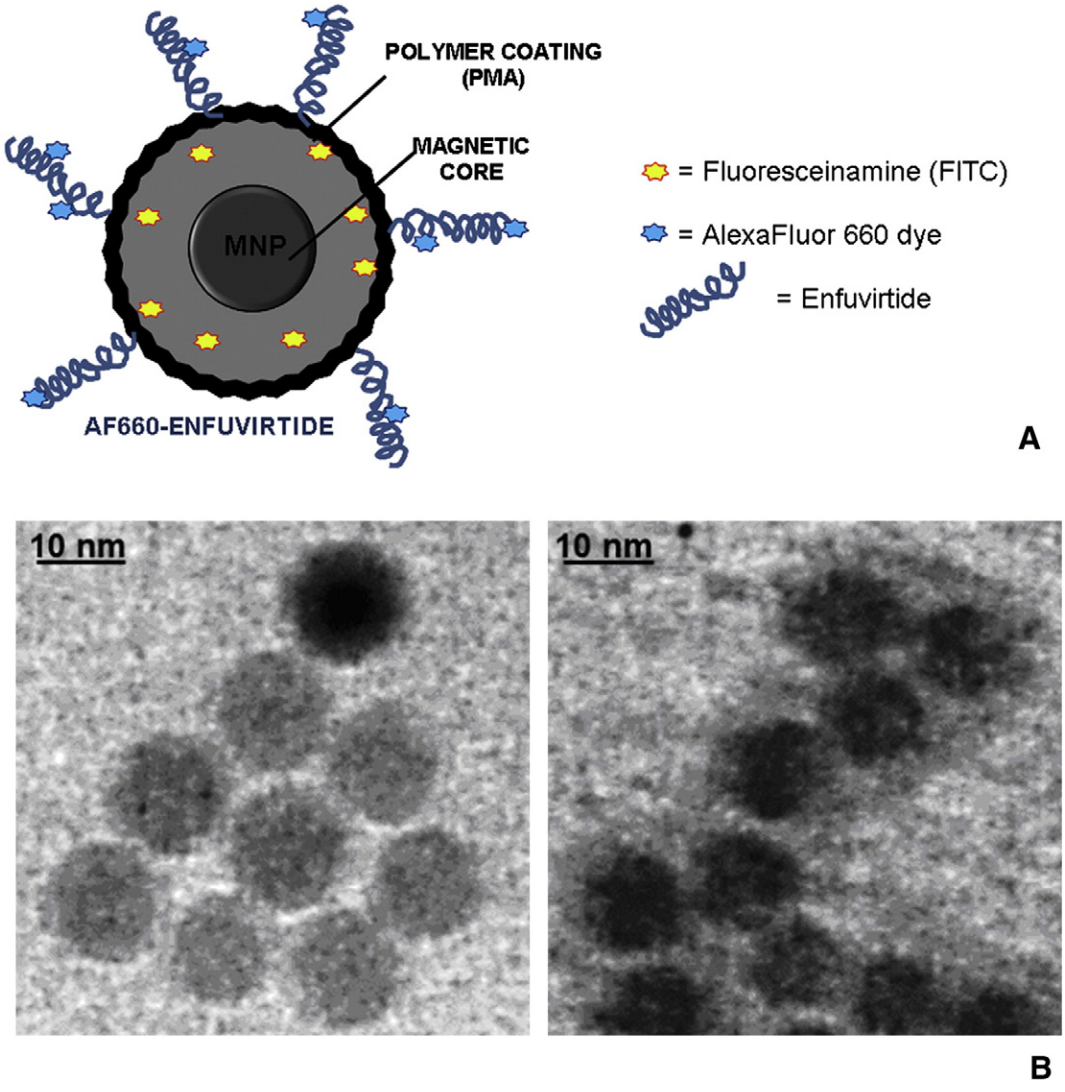

Figure 1. (**A**) Schematic representation of labeled Enf-MYTS. (**B**) TEM images of MNP in hexane (left) and MYTS in water (right).

animals per experimental condition). The amount of injected Enf-MYTS was calculated normalizing the fluorescence intensity of conjugated Enf to that of the free peptide. After 30 min, 1 h and 6 h postinjection, blood was collected and its fluorescence intensity was determined spectrofluorimetrically. After subtraction of background fluorescence, determined in samples collected from mice before treatment, the amount of Enf was calculated by using a calibration curve with known amounts of the compounds dissolved in control plasma samples.

Ex vivo IVIS imaging

Mice injected with (AF660)Enf or (AF660)Enf-MYTS (three animals for each experimental group were employed in three different experiments, for a total of nine mice) were sacrificed 1 h after injection and dissected brains were analyzed in an IVIS Lumina II imaging system (Calipers Life Sciences, UK), together with the brains from three non-treated mice. Images were acquired with a Cy5 emission filter, while excitation was scanned from 570 to 640 nm and tissue autofluorescence was removed by spectral unmixing.

Confocal laser scanning microscopy

For the confocal observations of brain cryosections, portions of the same tissues analyzed by IVIS or of additional tissues isolated from mice injected with 0.2 $\mu g\ g^{-1}$ body weight (AF660)Enf, or 12.5 $\mu g\ g^{-1}$ body weight (FITC)MYTS, (AF660)Enf-MYTS or (AF660)Enf-MYTS(FITC) (three animals for each experimental group), were fixed, freezed in liquid nitrogen and cryosectioned. Cryosections were counterstained with DAPI and NeuroTrace 530/615 fluorescent Nissl stain or immunodecorated with anti-CD31.

For the confocal microscopy of RBMVECs (three inserts for each experimental condition), cells on insert were fixed and immunodecorated with anti-CD31 and DAPI.

Images were acquired by a Leica TCS SPE confocal microscope and the intracellular distribution of AF660 and FITC signals was analyzed by ImageJ software.

Each image is representative of at least six images obtained from three inserts or mice brain sections for each experimental condition.

Scanning and transmission electron microscopy

For TEM analysis, MYTS were dispersed under sonication in water (50 μg mL^{-1}) and a drop of the resulting solution was placed on a formvar/carbon-coated copper grid and air-dried.

RBMVECs layered on inserts and exposed or not to 0.1 mg Enf-MYTS or MYTS, and sections of mice brains, exposed *in vivo* to the same nanoformulates (12.5 μg g^{-1} body weight), were analyzed by TEM, by fixing small portions of cells-bearing inserts (n = 3) or tissues (pieces obtained from the same brains employed for confocal microscopy analyses) in 2.5% glutaraldehyde. For scansion electron microscopy analyses, other small portions of the RBMVECs-bearing inserts were fixed and processed as described in Supplementary materials.

Histopathology

Brain, liver, kidneys, spleen and lung samples obtained from three Balb/c mice, whose brains were analyzed by confocal microscopy, were fixed in 10% buffered formalin for at least 48 h and embedded in paraffin. Three μm sections were cut, stained with hematoxylin and eosin and examined blindly.

Statistical analysis

All mean values ± SE reported in Results section and in Supplementary materials were compared by Student's *t* test.

Results

Nanoparticle characterization

MNP and the final Enf-MYTS, synthesized as described in Methods and Supplementary materials, were characterized in size and shape by DLS and TEM (Figure 1, *B*). MNP had a hydrodynamic diameter of 18.8 nm ± 2.1 in hexane. After the phase transfer, MNP maintained the original average crystal size (8 nm by TEM), and the final nanoparticle shape was uniformly spherical, with a hydrodynamic diameter of 23.9 ± 2.0 nm (MYTS in water) as determined by DLS. After drug conjugation, the nanoparticle size increased up to 35.2 ± 2.2 nm. The pH value of the suspension was around 5.5 and the zeta potential obtained at this pH value was −29.58 ± 1.90 mV, likely suggesting a high stability of Enf-MYTS with minimal aggregation in water medium at this pH. Indeed a zeta potential value higher than ±30 mV is generally required for a colloidally stable nanoparticle dispersion.[26,27]

Nanoconjugated enfuvirtide crosses the in vitro BBB model

The efficiency of MYTS in increasing the trans-BBB permeation of Enf was first evaluated on an *in vitro* BBB model consisting of a double layer of astrocytes and RBMVECs. Before treatment, the integrity of our experimental model was validated by measuring TEER and by determining the trans-BBB apparent permeability of the Dextran 40. In all BBB models devoted to the subsequent experimental phase, we recorded a mean TEER value higher than 400 Ω cm^2. BBB selectivity to the Dextran 40 labeled with FITC (FD40) was assessed in some additional inserts by measuring the trans-BBB flux over 3 h (Figure S1). The resulting P_{app} ($0.10 \pm 0.03 \times 10^{-7}$ cm s^{-1}, mean ± SE, n = 6) confirmed the production of a very tight barrier. SEM observations showed the presence of a uniform layer of endothelial cells (Figure S2A), and TEM images clearly demonstrated that cells were connected by well-structured tight junctions (Figure S2B).

The permeability of Enf, MYTS and Enf-MYTS across the BBB model was determined by labeling the peptide and the nanoparticle with AF660 and FITC, respectively (Figure 1, *A*). The nanoparticle suspensions were added in the upper chamber of the experimental apparatus and their passage through the BBB model was assessed after 4 and 7 h of incubation by measuring their fluorescence intensity (FI) into the lower chamber. We found that only a small fraction of free Enf was able to cross the BBB *in vitro*: after 4 h, Enf FI in the lower chamber was about 0,15 % of Enf FI added in the upper chamber, and the percentage increase of FI in the lower chamber over the subsequent 3 h of incubation was 30% (Figure 2, *A*). Conjugation of Enf to the nanoparticle did not significantly affect its FI in the lower chamber within the first four hours, but it was able to greatly increase its permeation across the BBB (by over 170%) between 4 and 7 h of incubation (Figure 2, *A*). Surprisingly, the percentage increase of the FITC FI in the lower chamber calculated between 4 and 7 h, which is associated to MYTS permeation across the BBB, was only 10%, and therefore much lower than that of the conjugated peptide in the same time span (Figure 2, *B*). The great difference between the % increase in lower chamber of AF660 (conjugated to Enf) and FITC (conjugated to MYTS) after incubation with the Enf-MYTS nanocomplex strongly suggested that the two components did not have the same fate when crossing the BBB, and that they likely dissociated into the barrier to be processed separately. The permeation of MYTS through the BBB was also assessed by measuring the iron content in the solution collected by the lower chamber by ICP-OES: we found that the percentage increase of iron recorded between 4 and 7 h was only 1.84 ± 0.04 (mean ± SE, n = 8) for both MYTS and Enf-MYTS.

Then, we measured the FI of the three formulations in the lower chamber of the BBB apparatus after 24 h of incubation. We observed that the Enf trans-BBB permeation was enhanced between 7 and 24 h of incubation by 175% (Figure 2, *A*), likely because of increased leakage of the RBMVEC barrier over the time. However, the effect of the nanocomplexation on the permeation of Enf across the BBB was still remarkable: the percentage increase of AF660 FI in the lower chamber between 7 and 24 h of exposure to Enf-MYTS reached 745% (Figure 2, *A*). By contrast, the percentage increase of FITC FI in the lower chamber was about 20% for both MYTS and Enf-MYTS (Figure 2, *B*), thus underlining a discrepancy between the FI recorded for Enf and MYTS after incubation of the BBB with Enf-MYTS. The percentage increase of iron content in the lower chamber between 7 and 24 h was still negligible and comparable for both conjugated and unconjugated nanoparticles (1.89% ± 0.03, mean ± SE, n = 8).

In parallel, we performed a confocal microscopy analysis of the upper side of the insert after 7 h of incubation with Enf or

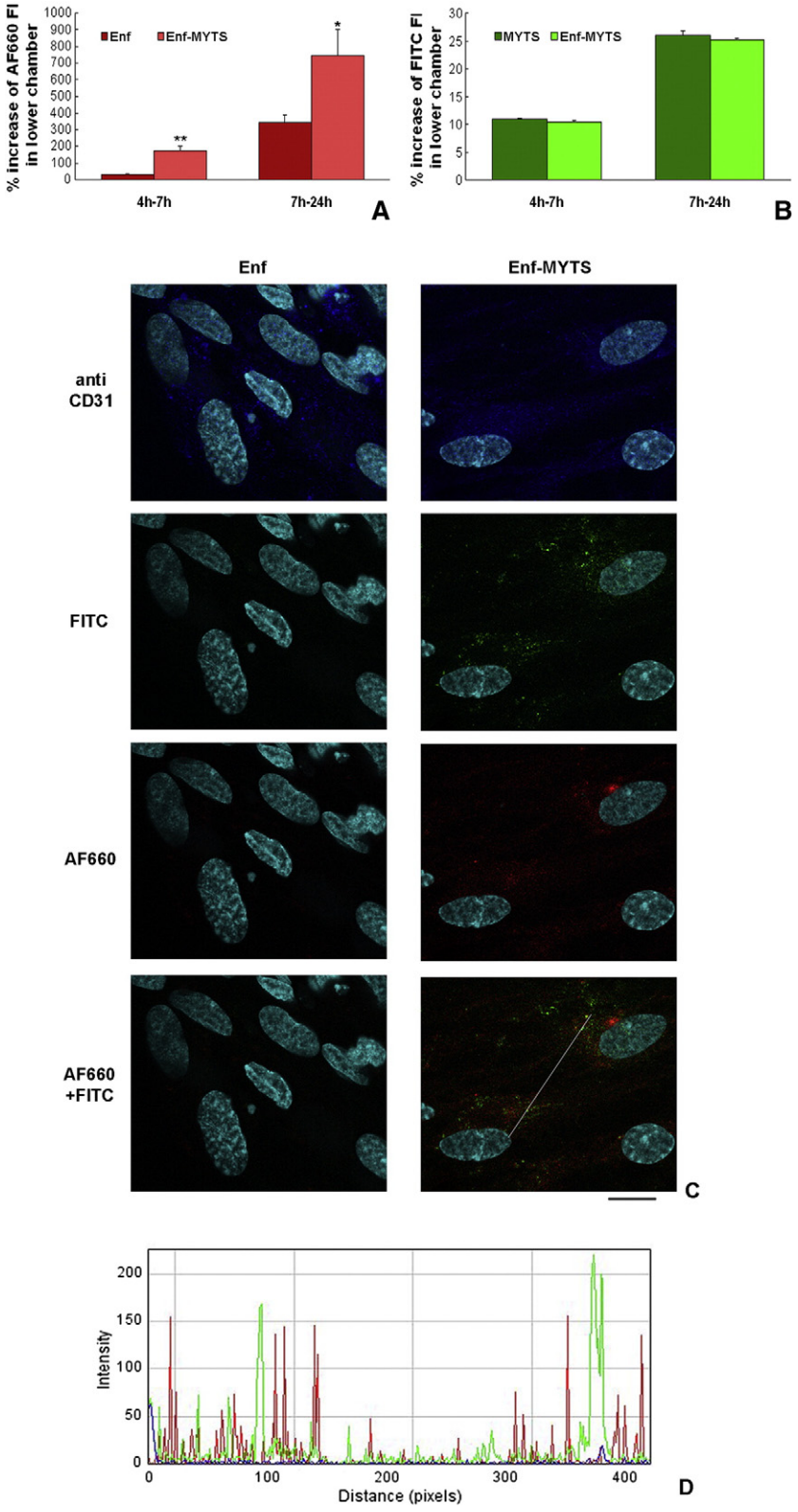

Figure 2. Percentage (%) increase of FI of free or conjugated (AF660)Enf (**A**) or (FITC)MYTS (**B**) in the lower chamber of the BBB *in vitro* system calculated between 4 and 7 h, and 7 and 24 h, from the addition of labeled Enf, MYTS and Enf-MYTS into the upper chamber. Mean ± SE of 4 replicates; $^{**}P < 0{,}001$ and $^{*}P < 0{,}05$, Enf-MYTS vs Enf (Student's *t* test) (**C**) Confocal laser-scanning micrographs (single optical sections) of RBMVECs after 7 h of incubation with free Enf or Enf-MYTS. Enf and MYTS are labeled with AF660 (red) and FITC (green) respectively; nuclei are stained with DAPI (cyan) and endothelial cells are immunodecorated with anti-CD31 antibody (blue); scale bar: 10 μm. (**D**) Overlay of the signal intensity plots of Enf and MYTS along a one-pixel line covering a cytoplasmic portion of the cells.

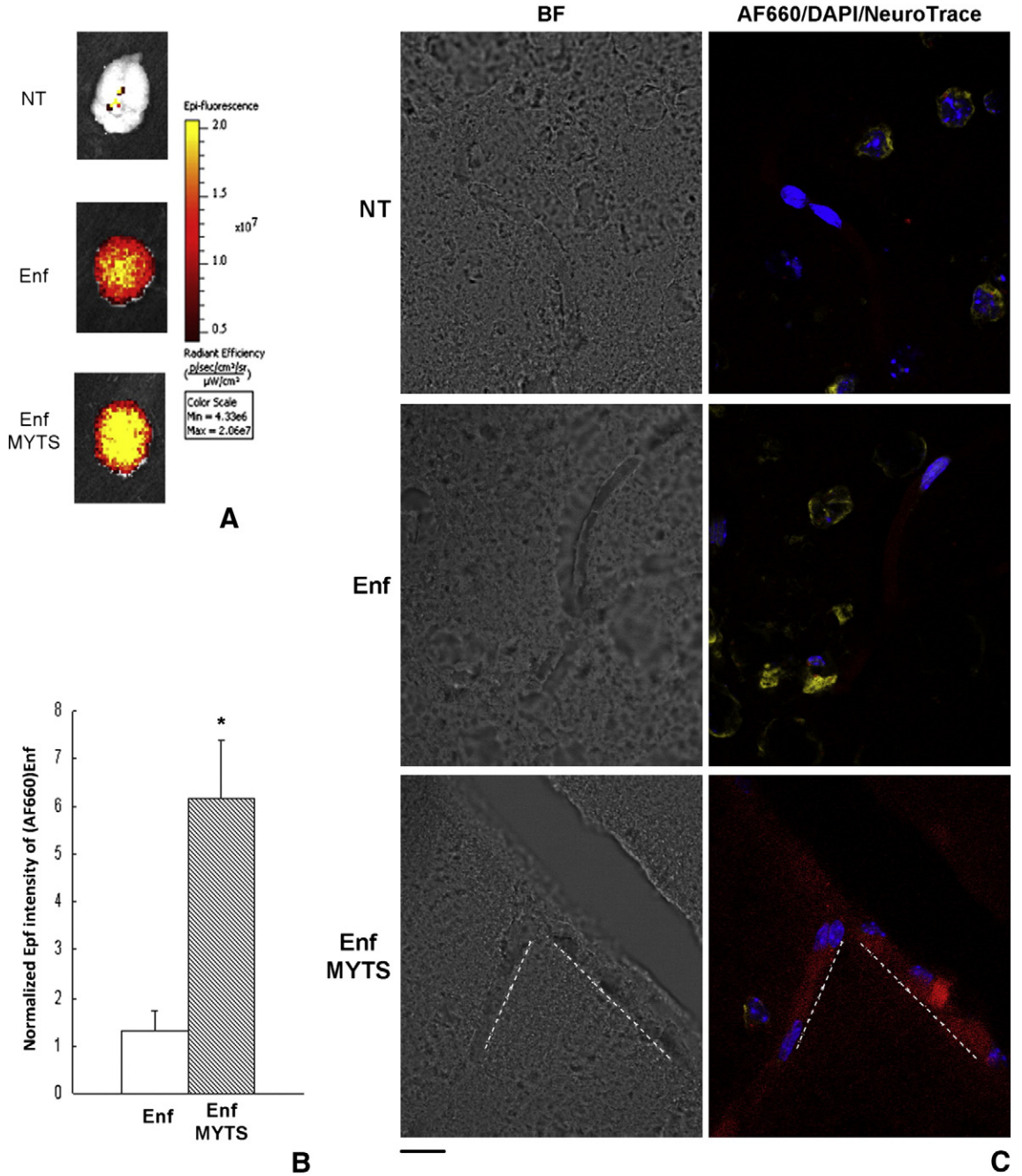

Figure 3. Analysis of brains isolated from non-treated mice (NT) or mice exposed for 1 h to free or conjugated AF660-labeled enfuvirtide. (**A**) Epf images of isolated brains, where Epf intensity is expressed as radiant efficiency. (**B**) Averaged Epf intensity of isolated brains where Epf values have been normalized on fluorescence intensity of injected solution in order to keep into account the differences in intrinsic fluorescence emission for each preparation; mean ± SE of 9 different brains for each experimental condition; *$P < 0{,}01$ (Student's t test). (**C**) Confocal laser-scanning micrographs (single optical sections) of brain cryosections; images from control animals (NT) or from animals treated with free or nanocomplexed enfuvirtide (red) have been overlaid on the corresponding images reporting nuclei (blue) and neuronal cytoplasm (yellow), counterstained with DAPI and NeuroTrace 530/615, respectively (right column); brightfield (BF) images are reported on the left; dashed lines highlight the vessel boundaries; bar: 10 µm.

Enf-MYTS. Figure 2, *C* shows that while free Enf was not internalized by the RBMVECs, the conjugation of the peptide to the nanoparticles allowed it to deeply enter into the cells, confirming the enhanced permeability of Enf when nanoconjugated. The merge image of the cells incubated with Enf-MYTS revealed that the AF660 and the FITC fluorescence were mostly non-overlapping (Figure 2, *C* and D). These image data, combined with the great difference in the trans-BBB permeation rate observed between the two components, strongly suggested that a dissociation of the peptide from the nanoparticle might have occurred in the endothelial layer.

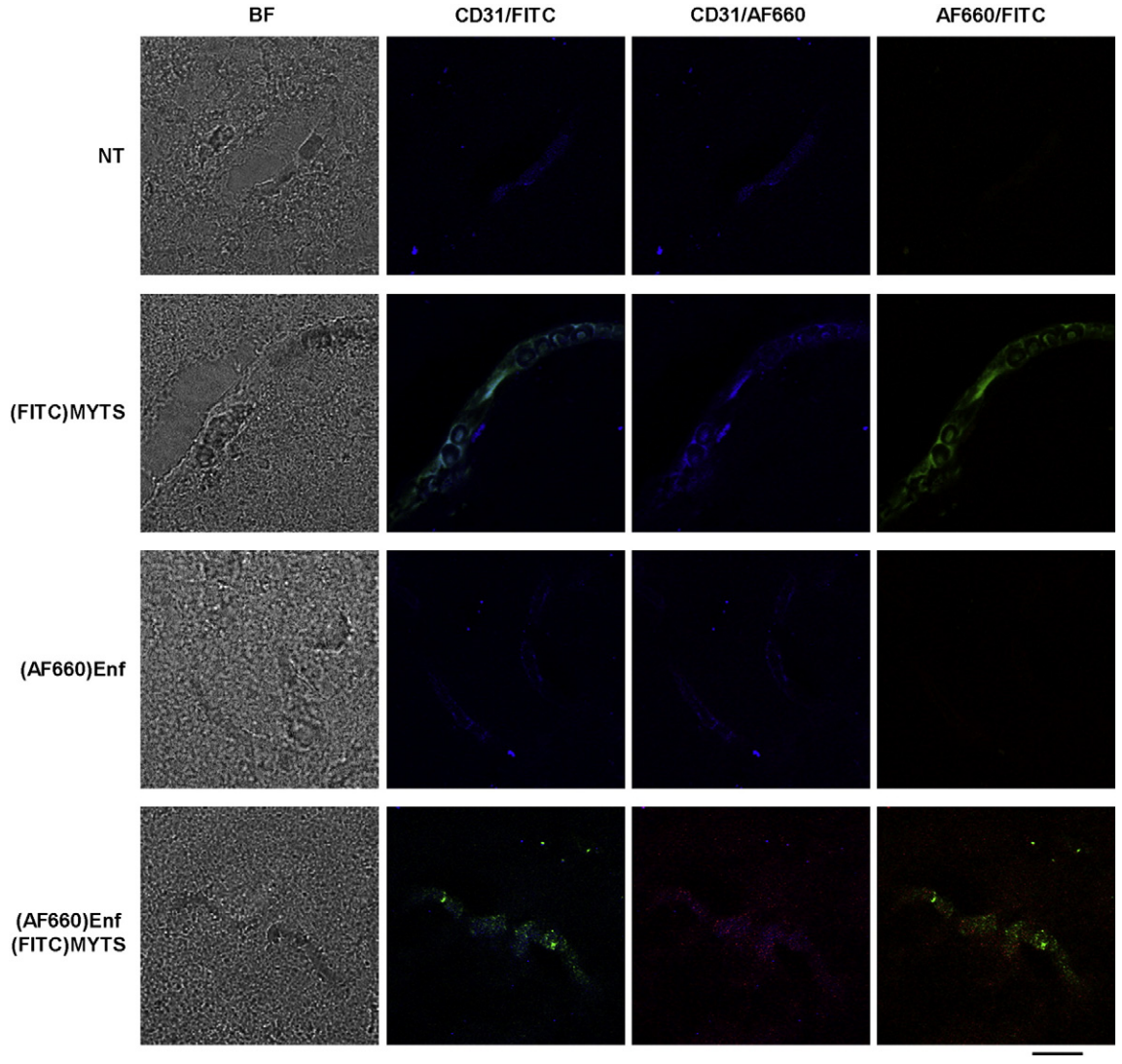

Figure 4. Confocal laser-scanning micrographs (single optical sections) of brain cryosections from non-treated mice (NT) or mice exposed for 1 h to (AF660)Enf, (FITC)MYTS or (AF660)Enf-MYTS(FITC); conjugated or free AF660-Enf (red) and FITC-MYTS (green) have been overlaid each other and with CD-31 stained endothelial cells (blue); brightfield (BF) images are reported on the left; bar: 10 μm.

In vivo brain targeting and trans-BBB delivery of nanoconjugated enfuvirtide

Trans-BBB permeation of MYTS-conjugated Enf was then assessed *in vivo* in Balb/c mice intravenously injected with free Enf or with the same peptide conjugated to nanoparticles. We decided to follow the bioavailability and biodistribution of Enf, by labeling the peptide with AF660 whose efficiency as *in vivo* probe had been previously reported in mice.[28,29] Firstly, plasma concentration of free or conjugated Enf was monitored at 30 min, 1 h and 6 h after injection in eight different animals for each experimental condition, to verify the effect of nanoconstruct on peptide bioavailability. We observed a maximal concentration of both free or conjugated drug in the blood stream within 1 h postinjection and a strong decrease over the following hours, up to negligible levels at 6 h postinjection. Moreover, Enf concentration in plasma appeared reduced by conjugation to MYTS and therefore less available for the potentially infected organs, including brains (Figure S3). Other mice were injected with Enf or Enf-MYTS (nine for each experimental condition) to be sacrificed at 1 h postinjection, together with three untreated animals (controls). Fluorescence imaging of dissected brains revealed a significant accumulation of both free and nanoformulated Enf in this organ at 1 h postinjection, as pointed out by the strong Epf signal not observed in the brain of non-treated mice (Figure 3, *A*), feasibly due to the peptide content in the blood circulation of brain. Neverthless, Epf intensity associated with nanoformulated Enf was stronger than that of free Enf (Figure 3, *A, B*), thus suggesting a higher accumulation of the nanoformulated peptide in this organ despite its lower bioavailability. To determine if the observed increased concentration of Enf in the brain was really associated to an increased permeation of the drug across BBB by effect of the nanocomplexation, we analyzed the interaction of Enf and Enf-MYTS with BBB cells and their localization in the

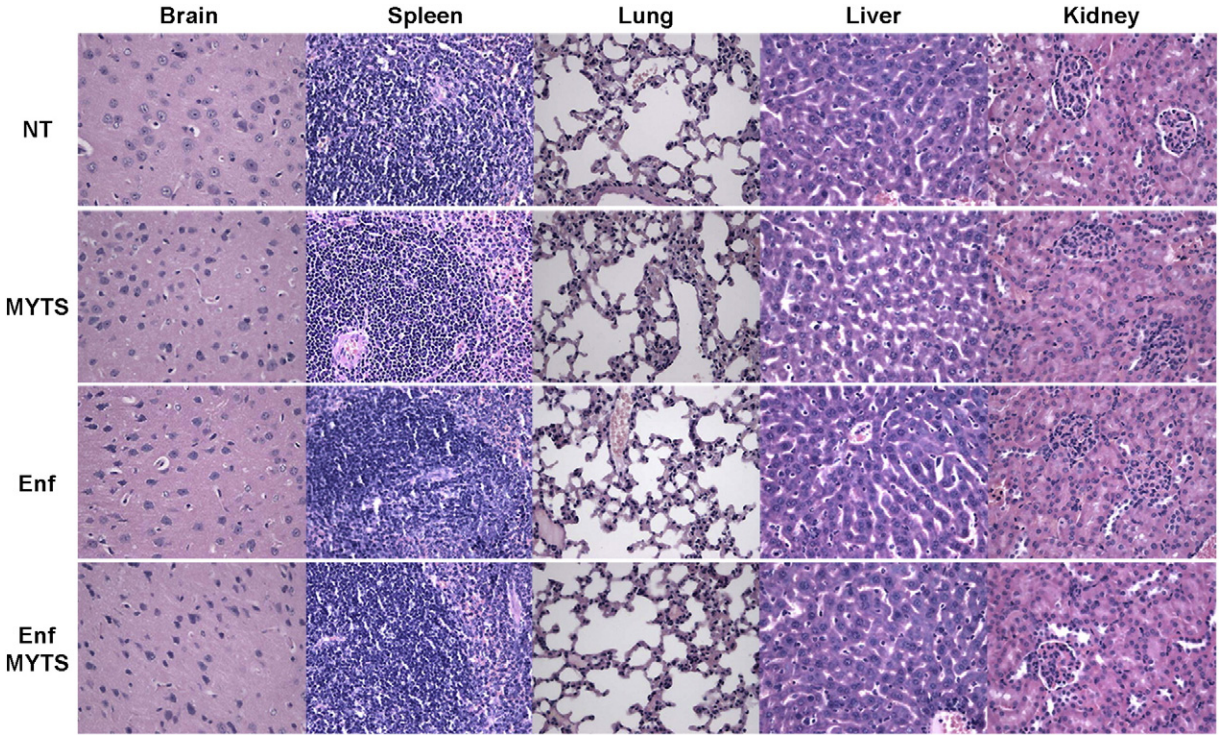

Figure 5. Histopathological analysis of brain, spleen, lung, liver and kidney dissected from non-treated (NT) mice, or from mice injected with MYTS, Enf and Enf-MYTS. Hematoxylin-eosin, OM ×40.

perivascular space. Cryosections of mice brains excised 1 h postinjection of Enf or Enf-MYTS were analyzed by confocal microscopy. Figure 3, *C* shows enhanced fluorescence intensity in brain capillaries in samples treated with the nanoconjugated Enf when compared to the free peptide, where instead fluorescence was only slightly higher than control autofluorescence. In addition, nanocomplexation of Enf induced a spreading of fluorescence outside the boundaries of the vessel.

To confirm the efficacy of MYTS in driving Enf into the endothelial cells of brain capillaries and finally exerting an efficient trans-BBB permeation of the drug, we injected mice with MYTS, Enf or Enf-MYTS (three mice for each experimental condition) and analyzed the localization of the different compounds in brain sections after 1 h from injection, by means of the differential labeling of Enf and MYTS with AF660 and FITC, respectively (Figure 4). Immunodecoration of the endothelial cells with anti-CD31 antibody revealed a huge intracellular accumulation for MYTS. As expected, the ability of free Enf to enter BBB endothelial cells and reach brain parenchyma was negligible, while conjugation of the peptide to the nanoparticles allowed it to cross the barrier. Merge between Enf and MYTS signals in samples treated with Enf-MYTS clearly showed that only the peptide was able to diffuse outside the BBB, while nanoparticles were restricted to the vessel endothelium. This result, in agreement with *in vitro* observations, further suggested the dissociation of the nanocomplex within endothelial cells, with subsequent excretion of Enf.

The systemic toxicity of administered formulations was then assessed by histopathological examination of brain, liver, kidneys, spleen, and lungs isolated 1 h after Enf, MYTS or Enf-MYTS injection. Analysis was performed on organs specimens from three different animals for each experimental condition. No histological lesions were observed in the analyzed organs (Figure 5).

Fate of MYTS in RBMVECs

The mechanism of MYTS entry and trafficking into the RBMVECs was investigated by TEM analysis on BBB-bearing inserts after 4, 7 or 24 h from the addition of Enf-MYTS in the upper chamber. Figure 6, *A* shows that, at 4 h of incubation, nanoparticles were either attached to the plasma membrane of the endothelial cells or internalized in the cytosol. The lack of membrane invaginations and the presence of free nanoparticles in the cytoplasm suggest that a non-endocytotic mechanism is involved in the internalization of MYTS by RBMVECs, as confirmed also by TEM images of brain samples exposed *in vivo* to the nanocomplex (Figure S4). Macropinocytosis rafts were also visible where a large number of nanoparticles came in contact with the cellular membrane. Once internalized, MYTS accumulated into large cellular compartments (Figure 6, *A* and *B*), and after 24 h of incubation, they were also detected into lysosomes (Figure 6, *C*). The same result was obtained by incubating the cells with the unconjugated MYTS.

Discussion

The BBB is the boundary that isolates brain tissues from the substances circulating in the blood and at the same time allows water and small lipophilic molecules to freely access the brain in

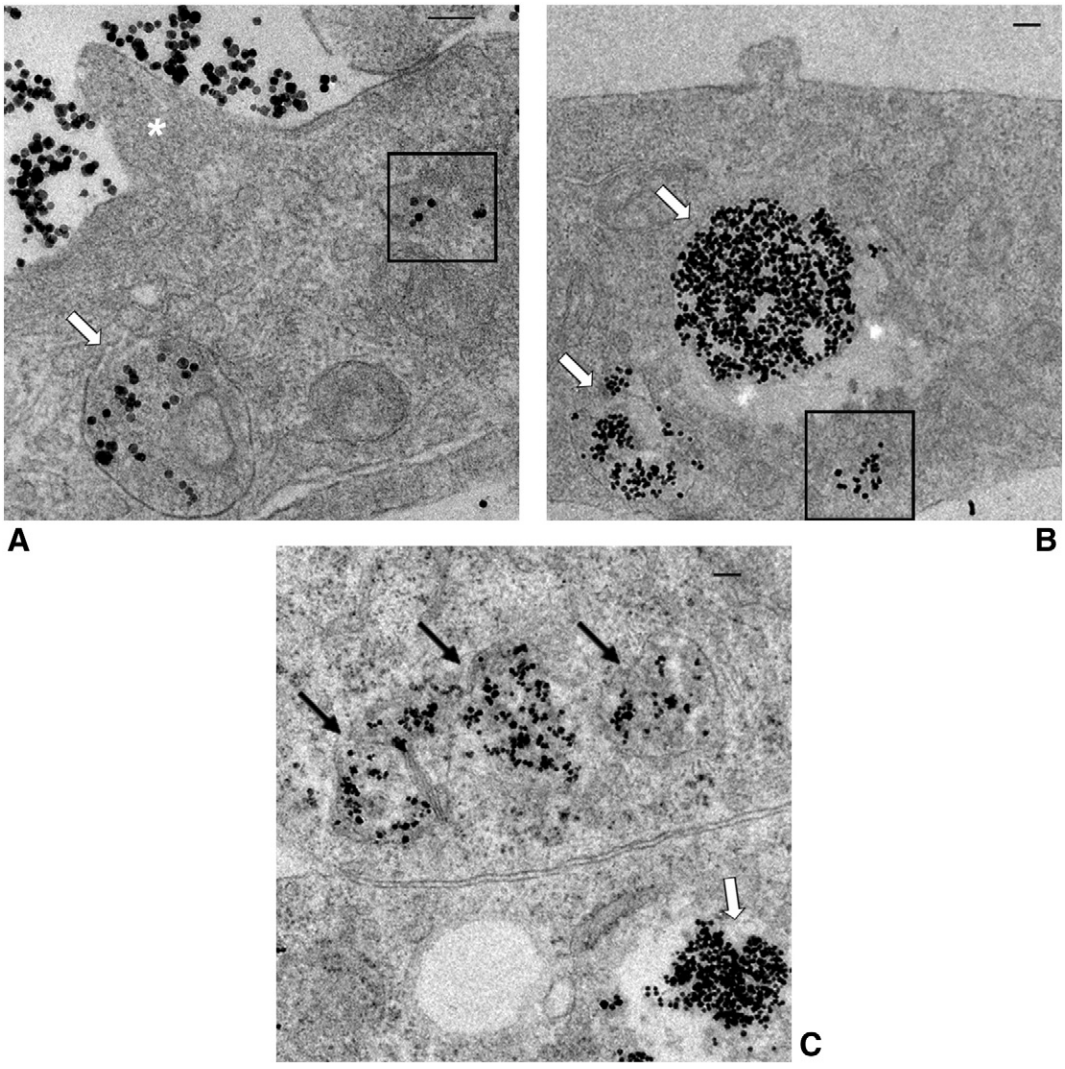

Figure 6. TEM images of RBMVECs in a BBB *in vitro* model exposed to 0.1 mg Enf-MYTS for 4 h (**A**), 7 h (**B**) and 24 h (**C**). MYTS are localized in big cell compartments (white arrows), in lysosomes (black arrows) or free into the cytosol (boxes); asterisk indicates a macropinocytosis raft; bars: 100 nm.

accordance with their concentration gradients. Within this barrier, the brain microvascular endothelial cells, phenotypically different from the endothelial cells of the peripheral circulation, hamper the filtration of therapeutic drugs, preventing them to reach the pathological tissues behind them. To permeate through the BBB, molecules need to be lipid soluble with a molecular weight <400 Da. Heavier and larger molecules, which are unable to diffuse through the BBB because of their size, weight and/or polarity, could cross the BBB only if transported by receptor-mediated transcytosis using ligands that bind specific BBB receptors. Therefore, drugs permeability across the BBB represents a clinical and biological challenge.

It is well established that a double correlation between HIV infection and the brain exists: HIV replication plays a major role in neurological diseases, and CNS is one of the main viral reservoir. During the acute phase of infection, HIV-1 rapidly infiltrates the CNS; there the viral replication can occur despite a complete drug-induced suppression of the virus in the peripheral blood. Noteworthy, while about 50% of HIV-infected patients are affected by neurological disease, evident morphological alterations in CNS are observed in at least 80% of AIDS patients autopsies.[30] The acclaimed model for HIV-related injury of CNS involves the release from infected or activated glial cells (microglia and astrocytes) of numerous neurotoxic viral or cellular factors, which lead to neuronal damage and death, and of chemoattractants able to promote infiltration of infected and/or activated monocytes.[4]

In NeuroAIDS prevention, nanotechnology has been intensely explored with the aim to develop novel and promising drug delivery systems, and several experimental attempts have been carried out in last years in order to enhance the BBB permeability toward antiretroviral drugs. Indeed, BBB has been demonstrated to be impermeable to 98% of antiretroviral drugs.[31] In 2006, Kuo and colleagues have incorporated two antiretroviral drugs, zidovudine and lamivudine, into polymeric polybutylcyanoacrylate (PBCA) nanoparticles, showing a 8-20 and 10-18 fold increase in BBB permeation, respectively.[32] However, polymeric nanoparticles are not suitable as carriers for polar or ionic drugs, and degradation of PBCA can produce toxic formaldehyde by-products.[31] Other biocompatible polymers, such as

polylactide, have been studied as novel nanocarriers for CNS drug delivery, but a transient inflammatory response has been reported.[31] Conjugation of the protease inhibitor saquinavir with transferrin-conjugated quantum dots has shown improved BBB penetration *in vitro*, by exploiting an active transport mechanism mediated by transferrin receptors; nevertheless, *in vivo* results are still missing.[14] Other nanocarriers such as liposomes are inefficient for loading with water-soluble drugs.[31]

In our study we have designed and developed a novel nanodrug consisting of an iron oxide nanoparticle coated with a suitable amphiphilic polymer and functionalized with the antiretroviral peptide enfuvirtide. Although rarely used in clinical practice, we selected Enf for two main reasons. First, it has proven effective as a non-selective inhibitor of HIV-1 fusion with cells, able to preclude virus entry regardless its co-receptor tropism. The blockade of virus entry into cells is relevant in view of the use of drugs that purge the latent reservoir, damming the circulating HIV-1 pool of virus that should not re-infect new cells. Secondly, Enf is one of the most structurally complex antiretroviral molecules, therefore ideal for testing the efficacy of our nanoconstruct as a drug delivery system to the brain.

So far, the use of iron oxide nanoparticles as antiretroviral carriers has been poorly investigated *in vivo*.[31] In the present work, our polymer-coated iron oxide nanoparticles (namely MYTS) have proven to be promising as CNS drug delivery system for antiretroviral drugs, by taking advantage of their intrinsic propensity to cross the BBB. We observed *in vitro* an increased permeation of nanoformulated Enf across BBB up to 170% upon 3 h of incubation. Moreover, conjugated Enf showed increased epifluorescence intensity in mice brain, as a result of its huge CNS accumulation. Electron microscopy images suggested that endocytosis is not likely responsible for the internalization of MYTS in the endothelial cells, even though the presence of a large number of nanoparticles on the cell surface activated the production of macropinocytosis membrane ruffles. Rather, the presence of free nanoparticles in the cell cytoplasm strongly suggests that their internalization mainly occurred by a passive diffusion, probably mediated by the absorption of the amphiphilic coating on the cell membrane. In previous studies, it has been assumed that polymer aggregates carrying hydrophobic groups should have the same affinity for brain endothelial cell membranes of pluronic block copolymers[33], whose absorption on cell membrane induces a structural alteration of the lipid bilayer.[34] Membrane fluidization allows the pluronics micelles to enter the microvessel endothelial cells and deliver their cargo into the intracellular environment.[34] Once into the cell, MYTS were sequestered by huge endosome-like compartments and then directed to lysosomes. Our data indicate that Enf dissociated from MYTS in the endothelial cells to be efficiently excreted into the outside environment. The dissociation mechanism requires further studies to be elucidated, but it could involve the degradation of the PMA shells bearing the peptide. PMA degradation feasibly started into the more mature endosomal compartments, as an effect of the increased acidity and enzymatic activity of their inner environment, to be then completed within lysosomes. Concerning Enf efflux, it is known that foreign substances are usually rejected by the BBB through an efflux mechanism based on transporters such as P-glycoprotein and multidrug resistance-associated protein (MRP).[35] The brain-directed efflux of Enf could occur via MRP4, a protein expressed on the abluminal membrane of the brain capillary endothelial cells, which were proven to mediate the excretion of different drugs, including some antiretrovirals.[36] Histopathological analysis of brain, spleen, lung, liver and kidneys dissected from mice upon Enf treatment, confirmed that this antiretroviral drug does not exert toxic effects. Moreover, the lack of any organ lesion in the presence of circulating MYTS is a clear evidence of the systemic safety of these nanoparticles at the experimental dosage, further supporting their great potential as drug delivery system across the BBB.

In conclusion, this is the first documented experience of a nanotechnological engineering of the complex antiretroviral drug enfuvirtide, which confers to this large peptide the capability to cross the BBB. Whether and how the propensity of Enf nanoconjugate to cross the BBB could affect the viral replication in the CNS sanctuary remain to be established, and further studies will be performed to assess the antiviral efficacy of Enf after trans-BBB permeation. However, at present, our results represent an important step forward toward HAART-mediated HIV eradication from the CNS reservoir. Since MYTS nanoparticles can be loaded with multiple drugs of different classes, the present study suggests a straightforward approach for targeting various phases of viral replication in the CNS.

Appendix A. Supplementary data

Supplementary data to this article can be found online at http://dx.doi.org/10.1016/j.nano.2015.03.009.

References

1. Sarmati L, Parisi SG, Montano M, Andreis S, Scaggiante R, Galgani A, et al. Nevirapine use, prolonged antiretroviral therapy and high CD4 nadir values are strongly correlated with undetectable HIV-DNA and -RNA levels and CD4 cell gain. *J Antimicrob Chemother* 2012;**67**:2932-8.
2. Cory TJ, Schacker TW, Stevenson M, Fletcher CV. Overcoming pharmacologic sanctuaries. *Curr Opin HIV AIDS* 2013;**8**:190-5.
3. Bunupuradah T, Bowonwattanuwong C, Jirajariyavej S, Munsakul W, Klinbuayaem V, Sophonphan J, et al. HIV-1 genital shedding in HIV-infected patients randomized to second-line lopinavir/ritonavir monotherapy versus tenofovir/lamivudine/lopinavir/ritonavir. *Antivir Ther* 2014;**24**, http://dx.doi.org/10.3851/IMP2737.
4. Kramer-Hämmerle S, Rothenaigner I, Wolff H, Bell JE, Brack-Werner R. Cells of the central nervous system as targets and reservoirs of the human immunodeficiency virus. *Virus Res* 2005;**11**:194-213.
5. Surdo M, Cortese MF, Perno CF, Aquaro S. NeuroAIDS: virological aspects of HIV infection. *J Biol Regul Homeost Agents* 2013;**27**:115-28.
6. Doyon G, Sobolewski MD, Huber K, McMahon D, Mellors JW, Cremer NS. Discovery of a small molecule agonist of phosphatidylinositol 3-kinase p110α that reactivates latent HIV-1. *PLoS One* 2014;**29**, http://dx.doi.org/10.1371/journal.pone.0084964.
7. Wightman F, Lu HK, Solomon AE, Saleh S, Harman AN, Cunningham AL, et al. Entinostat is a histone deacetylase inhibitor selective for class 1 histone deacetylases and activates HIV production from latently infected primary T cells. *AIDS* 2013;**27**:2853-62.
8. Shan L, Xing S, Yang HC, Zhang H, Margolick JB, Siliciano RF. Unique characteristics of histone deacetylase inhibitors in reactivation of latent HIV-1 in Bcl-2-transduced primary resting CD4+ T cells. *J Antimicrob Chemother* 2014;**69**:28-33.

9. Kent SJ, Reece JC, Petravic J, Martyushev A, Kramski M, De Rose R, et al. The search for an HIV cure: tackling latent infection. *Lancet Infect Dis* 2013;**13**:614-21.
10. Parboosing R, Maguire GEM, Govender P, Kruger HG. Nanotechnology and the treatment of HIV infection. *Viruses* 2012;**4**:488-520.
11. Mamo T, Moseman EA, Kolishetti N, Salvador-Morales C, Shi J, Kuritzkes DR, et al. Emerging nanotechnology approaches for HIV/AIDS treatment and prevention. *Nanomedicine (Lond)* 2010;**5**:269-85.
12. Amiji MM, Vyas TK, Shah LK. Role of nanotechnology in HIV/AIDS treatment: potential to overcome the viral reservoir challenge. *Discov Med* 2006;**6**:157-62.
13. Mahajan SD, Aalinkeel R, Law WC, Reynolds JL, Nair BB, Sykes DE, et al. Anti HIV-1 nanotherapeutics: promises and challenges for the future. *Int J Nanomedicine* 2012;**7**:5301-14.
14. Mahajan SD, Roy I, Xu G, Yong KT, Ding H, Aalinkeel R, et al. Enhancing the delivery of anti retroviral drug "saquinavir" across the blood brain barrier using nanoparticles. *Curr HIV Res* 2010;**8**:396-404.
15. Trottier B, Walmsley S, Reynes J, Piliero P, O'Hearn M, Nelson M, et al. Safety of enfuvirtide in combination with an optimized background of antiretrovirals in treatment-experienced HIV-1-infected adults over 48 weeks. *J Acquir Immune Defic Syndr* 2005;**40**:413-21.
16. Liu S, Lu H, Niu J, Xu Y, Wu S, Jiang S. Different from the HIV fusion inhibitor C34, the anti-HIV drug Fuzeon (T-20) inhibits HIV-1 entry by targeting multiple sites in gp41 and gp120. *J Biol Chem* 2005;**280**:11259-73.
17. Patel IH, Zhang X, Nieforth K, Salgo M, Buss N. Pharmacokinetics, pharmacodynamics and drug interaction potential of enfuvirtide. *Clin Pharmacokinet* 2005;**44**:175-86.
18. Dando TM, Perry CM. Enfuvirtide. *Drugs* 2003;**63**:2755-66.
19. Borrego P, Calado R, Marcelino JM, Bártolo I, Rocha C, Cavaco-Silva P, et al. Baseline susceptibility of primary HIV-2 to entry inhibitors. *Antivir Ther* 2012;**17**:565-70.
20. Sista P, Melby T, Greenberg ML, Davison D, Jin J, Mosier S, et al. Characterization of baseline and treatment-emergent resistance to T-20 (enfuvirtide) observed in phase II clinical trials: substitutions in gp41 amino acids 36-45 and enfuvirtide susceptibility of virus isolates. *Antivir Ther* 2002;**7**:S16-7.
21. Cilliers T, Patience T, Pillay C, Papathanasopoulos M, Morris L. Sensitivity of HIV type 1 subtype C isolates to the entry inhibitor T-20. *AIDS Res Hum Retroviruses* 2004;**20**:477-82.
22. Derdeyn CA, Decker JM, Sfakianos JN, Zhang Z, O'Brien WA, Ratner L, et al. Sensitivity of human immunodeficiency virus type 1 to fusion inhibitors targeted to the gp41 first heptad repeat involves distinct regions of gp41 and is consistently modulated by gp120 interactions with the coreceptor. *J Virol* 2001;**75**:8605-14.
23. Price RW, Parham R, Kroll JL, Baker B, Sailstad J, Hoh R, et al. Enfuvirtide cerebrospinal fluid (CSF) pharmacokinetics and potential use in defining CSF HIV-1 origin. *Antivir Ther* 2008;**13**:369-74.
24. Park J, An K, Hwang Y, Park JG, Noh HJ, Kim JY, et al. Ultra-large-scale syntheses of monodisperse nanocrystals. *Nat Mater* 2004;**3**:891-5.
25. Pellegrino T, Manna L, Kudera S, Liedl T, Koktysh D, Rogach AL, et al. Hydrophobic nanocrystals coated with an amphiphilic polymer shell: a general route to water soluble nanocrystals. *Nano Lett* 2004;**4**:703-7.
26. Bazylinska U, Kulbacka J, Wilk WA. Dicephalic ionic surfactants in fabrication of biocompatible nanoemulsions: factors influencing droplet size and stability. *Colloids Surf A Physicochem Eng Asp* 2014;**460**:312-20.
27. Alkilany AM, Abulateefeh SR, Mills KK, Bani Yaseen AI, Hamaly MA, Alkhatib HS, et al. Colloidal stability of citrate and mercaptoacetic acid capped gold nanoparticles upon lyophilization: effect of capping ligand attachment and type of cryoprotectants. *Langmuir* 2014;**30**:13799-808.
28. Zaharoff DA, Hance KW, Rogers CJ, Schlom J, Greiner J. Intratumoral immunotherapy of established solid tumors with chitosan/IL-12. *J Immunother* 2010;**33**:697-705.
29. Fiandra L, Mazzucchelli S, De Palma C, Colombo M, Allevi R, Sommaruga S, et al. Assessing the in vivo targeting efficiency of multifunctional nanoconstructs bearing antibody-derived ligands. *ACS Nano* 2013;**7**:6092-102.
30. De Almeida SM, Letendre S, Ellis R. Human immunodeficiency virus and the central nervous system. *Braz J Infect Dis* 2006;**10**:41-50.
31. Sagar V, Pilakka-Kanthikeel1 S, Pottathil R, Saxena SK, Nair M. Towards nanomedicines for neuroAIDS. *Rev Med Virol* 2014;**24**:103-24.
32. Kuo YC, Chen HH. Effect of nanoparticulate polybutylcyanoacrylate and methylmethacrylate-sulfopropylmethacrylate on the permeability of zidovudine and lamivudine across the in vitro blood–brain barrier. *Int J Pharm* 2006;**327**:160-9.
33. Hemmelman M, Knoth C, Schmitt U, Allmeroth M, Moderegger D, Barz M, et al. HPMA based amphiphilic copolymers mediate central nervous effects of domperidone. *Macromol Rapid Commun* 2011;**32**:712-7.
34. Batrakova EV, Li S, Vinogradov SV, Alakhov VY, Miller DW, Kabanov AV. Mechanism of pluronic effect on P-glycoprotein efflux system in blood-brain barrier: contributions of energy depletion and membrane fluidization. *J Pharmacol Exp Ther* 2001;**299**:483-93.
35. Demeule M, Regina A, Jodoin J, Laplante A, Dagenais C, Berthelet F, et al. Drug transport to the brain: key roles for the efflux pump P-glycoprotein in the blood–brain barrier. *Vascul Pharmacol* 2002;**38**:339-48.
36. Löscher W, Potschka H. Drug resistance in brain disease and the role of drug efflux transporters. *Nat Rev Neurosci* 2005;**6**:591-602.